

UCLA

UCLA Previously Published Works

Title

Mechanisms and Dynamics of Synthetic and Biosynthetic Formation of Delitschiapyrones:
Solvent Control of Ambimodal Periselectivity

Permalink

<https://escholarship.org/uc/item/1cr114vx>

Journal

Journal of the American Chemical Society, 143(30)

ISSN

0002-7863

Authors

Zou, Yike
Houk, KN

Publication Date

2021-08-04

DOI

10.1021/jacs.1c05293

Peer reviewed



HHS Public Access

Author manuscript

J Am Chem Soc. Author manuscript; available in PMC 2022 July 22.

Published in final edited form as:

J Am Chem Soc. 2021 August 04; 143(30): 11734–11740. doi:10.1021/jacs.1c05293.

Mechanisms and Dynamics of Synthetic and Biosynthetic Formation of Delitschiapyrones: Solvent Control of Ambimodal Periselectivity

Yike Zou,

Department of Chemistry and Biochemistry, University of California, Los Angeles, California 90095-1569, United States;

K. N. Houk

Department of Chemistry and Biochemistry, University of California, Los Angeles, California 90095-1569, United States;

Abstract

The mechanism and dynamics for the formation of the delitschiapyrone family of natural products are studied by density functional theory (DFT) calculations and quasiclassical molecular dynamics simulations with DFT and xTB. In the uncatalyzed reaction, delitschiapyrones A and B are formed by Diels–Alder reactions through a single transition state and a post-transition state bifurcation that favors formation of delitschiapyrone B. In water and most likely in the enzyme, the acidic hydroxyquinone ionizes, and the resulting conjugate base undergoes cycloaddition preferentially to delitschiapyrone A. We demonstrate a new type of biosynthetic transformation and variable selectivity from a (4 + 2)/(4 + 3) ambimodal transition state.

Graphical Abstract

Corresponding Authors: **Yike Zou** – Department of Chemistry and Biochemistry, University of California, Los Angeles, California 90095-1569, United States; zouyike@ucla.chem.edu, **K. N. Houk** – Department of Chemistry and Biochemistry, University of California, Los Angeles, California 90095-1569, United States; houk@ucla.chem.edu.

Supporting Information

The Supporting Information is available free of charge at <https://pubs.acs.org/doi/10.1021/jacs.1c05293>.

Computational details, Cartesian coordinates, and energies of all optimized structures and transition structures (PDF)

Neutral (4+2) pathway (Movie S1) (MP4)

Neutral (4+3) pathway (Movie S2) (MP4)

Anionic (4+2) pathway (Movie S3) (MP4)

Anionic (4+3) pathway (Movie S4) (MP4)

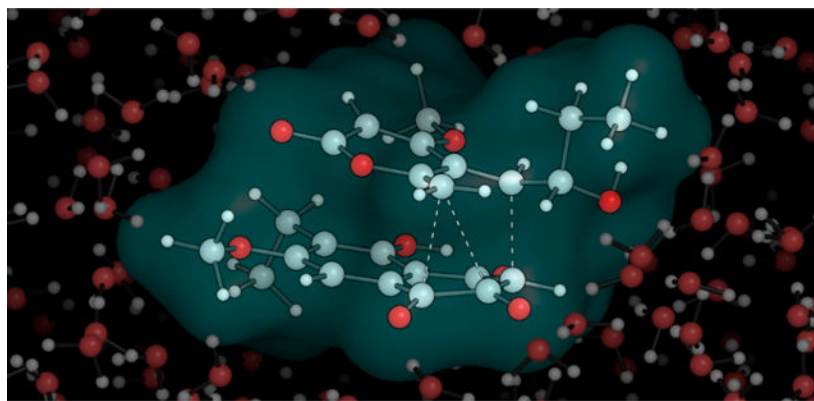
Anionic (4+2) pathway with explicit solvent model (Movie S5) (MP4)

Anionic (4+3) pathway with explicit solvent model (Movie S6) (MP4)

Complete contact information is available at: <https://pubs.acs.org/doi/10.1021/jacs.1c05293>

The authors declare no competing financial interest.

All DFT and xTB-MD calculations were performed using the Gaussian 09 program package.⁴⁹ Molecular dynamic simulations were performed using the ProgDyn program package^{50–52} with either Grimme's semiempirical xTB³ method with the GBSA solvation model with a Gaussian-xTB interface program⁵³ or a DFT method using ωB97X-D/6–31G(d,p) with the CPCM solvation model. Please find detailed computational procedures and various 1 ps MD simulation movies in the Supporting Information.



INTRODUCTION

Delitschiapyrone A (**1**) and B (**4**) are hybrid naphthoquinone/2-pyrone.¹ Both classes of natural products include potent drugs or drug candidates, as shown in Figure 1. The biosynthetic pathway that has been postulated¹ for formation of **4** involves an *exo* Diels–Alder reaction, while the formation of **1** involves a subsequent α -hydroxy ketone (α -ketol) rearrangement and cyclization (Figure 1a). Synthetically, **1** and **4** were made by a related process. The ratio of **1** and **4** was found to be solvent-dependent (Figure 1b).² We have studied these reactions with density functional theory (DFT) and quasiclassical molecular dynamics (MD) simulations with the xTB³ method and have discovered a novel mechanism that leads in one step to the skeletons of both **1** and **4**. We find that **1** and **4** are generated from a single reaction step involving a Diels–Alder/ α -ketol rearrangement or (4 + 2)/(4 + 3) ambimodal transition state. Delitschiapyrone B (**4**) is dynamically preferred for the neutral reactant, but ionization of the acidic hydroxyquinone moiety in water alters the dynamic preference to lead to delitschiapyrone A (**1**).

Naphthoquinones and 2-pyrones are formed from polyketide biosynthetic pathways.^{4–14} Representative members of these families of natural products include tetracycline, rifamycin, and solanapyrones.¹⁵ Delitschiapyrone A (**1**) is a naphthoquinone 2-pyrone hybrid first isolated from subtropic-plant-associated fungi collected in Florida.¹ Delitschiapyrone A (**1**) bears an unprecedented 6/6/5/7/6 pentacyclic multibridged ring system and displays bioactivities toward various human tumor cell lines *in vitro*. The proposed biosynthetic precursors **2** and **3** may react in an *exo* (4 + 2) fashion [assuming the (*Z*)-alkene is involved] leading to the formation of the tetracyclic ring system of delitschiapyrone B (**4**), which has not been isolated from cultures. An α -ketol rearrangement of **4** then permits ring expansion that forms the seven-membered ring of **5**. Enzymes that catalyze the (4 + 2) cycloaddition/ α -ketol rearrangement cascade are not known. Finally, an intramolecular hemiketalization/cyclization of **5** completed the proposed biosynthesis of delitschiapyrone A (**1**), with the structure confirmed by X-ray crystallographic analysis.¹ As shown from the XRD structure, delitschiapyrone A (**1**) possesses a strained ring system.

A biomimetic chemical synthesis of delitschiapyrone A (**1**) has been reported.² The key synthetic transformation is an *endo*-selective Diels–Alder reaction [of the (*E*)-

alkene]/ α -ketol rearrangement/cyclic-hemiketalization cascade leading to the formation of delitschiapyrone A (**1**) as the only stereoisomer as well as delitschiapyrone B (**4**), which was isolated and structurally characterized for the first time. Remarkably, all four additional consecutive stereogenic centers of **1** were constructed via asymmetric induction from the allylic stereo-center of **3**. Interestingly, change from a nonpolar solvent such as toluene to water leads to acceleration of the reaction and significantly increases the yield of **1**.

We are interested in elucidation of the mechanism of this transformation in both biological and abiological conditions as well as the origin of the stereoselectivity and the mechanism of water acceleration. There have been no previous mechanistic studies on the formation of a bicyclo[4.3.1]decane system from cycloadditions of a hydroxynaphthoquinone. Studies on an α -hydroxycarbonyl substrate were previously reported by our group: 2-hydroxyacrolein and 1,3-butadiene are predicted to give both a (4 + 2) and (4 + 3) + H shift from a single ambimodal transition state.¹⁶ An α -ketol rearrangement interconverts the two products. While that was a purely hypothetical reaction, we believe that nature uses a related reaction in the biosynthesis of delitschiapyrones A and B. We use ω B97X-D¹⁷ density functional theory to show that an ambimodal transition state and a post-transition state bifurcation^{18–23} leads to B (**4**) or a precursor (**5**) to A (**1**). Applying quasiclassical molecular dynamics (MD) simulation starting from the ambimodal (4 + 2)/(4 + 3) pericyclic transition state, we show the relationship of these two products and show how water solvation reshapes the potential energy surface. We have used the rapid semiempirical quantum mechanical method, xTB from Grimme,³ checked vs ω B97X-D for some cases. Water is known to accelerate various pericyclic reactions^{24–26} and to influence the α -ketol rearrangements²⁷ and other reactions by hydrogen-bond catalysis, polarity and surface effects.^{28,29}

RESULTS AND DISCUSSION

We initiated our studies with the cycloaddition transition states that lead to the (4 + 2) product **4**, which could be generated from either **3** or **6** depending on whether an *exo* or *endo* pathway is followed. We compute that the (*E*)-isomer is 1–2 kcal/mol more stable than the (*Z*). In the proposed biosynthetic pathway, the (4 + 2) cycloaddition of **2** with **3** proceeds with *exo* transition state **TS1-Z** and an energy barrier of 27.4 kcal/mol (Figure 2), although the exact configuration of the exocyclic double bond of **3** was not confirmed biosynthetically. By comparison, the energy barrier for the *endo* pathway of **2** with **6**, as proposed in the chemical synthesis, is lower (**TS1**, 21.9 kcal/mol), likely due to stabilizing secondary orbital interactions for **TS1** and the strong steric repulsions in **TS1-Z** arising from the diene planarity in the concerted transition state that always disfavors reactions of *Z*-dienes. Both transition states are asynchronous with C2–C19 as the first forming bond with a forming distance of 2.1 Å. Among all possible *endo* and *exo* stereoisomeric transition states, the *endo* transition states are in general approximately 6–10 kcal/mol lower in energy than the *exo* transition states.³⁰ **TS1** (**TS1-endo1** in Figure 3) has the lowest energy. The regioselectivity of **TS1-endo1** vs **TS1-endo3** can be rationalized by the larger frontier orbital coefficients at both C2 and C19 compared with C3 and C13, respectively. The facial selectivity of **TS1-endo1** is due to a preferred conformation of the C19 side chain with respect to the C2–C19 forming bond; in the favored transition state, the largest

alkyl group is *anti* to the forming bond, whereas for the other facial isomeric transition states (**TS1-endo2** and **TS1-endo4**), this conformation is no longer preferred; similar cases were studied extensively earlier.^{31–33} The orchestration of both orbital and steric interactions results in **TS1** as the favorable transition state that leads to the (4 + 2) product **4** that is thermodynamically downhill with a Gibbs free energy of -32.9 kcal/mol relative to the prereaction complex of **2** and **6**. Next, the α -ketol rearrangement proceeds with transition state **TS2** with a relative Gibbs free energy of 9.3 kcal/mol leading to ring expansion and product **5** with a free energy of -27.0 kcal/mol.

However, in order to generate **5** from **4**, an energy barrier of 42.2 kcal/mol must be overcome. Yet **5** is 5.9 kcal/mol less thermodynamically stable than **4**. These energetics indicate that **5** cannot be formed. However, a significant amount of **1** (spontaneous cyclization product of **5**) was isolated from both culture and reaction mixture.^{1,2} This disagreement between theory and experiment let us to postulate that the reaction must not proceed via the proposed cascade reaction pathway. Based on our previous studies, we propose here that the formation of **5** may not undergo a α -ketol rearrangement but instead directly from **2** and **6** via a single cycloaddition step. Although (4 + 2) was the major pathway in cases we previously studied, due to a post-transition state proton transfer that played an important role to slow down the (4 + 3) pathways,¹⁶ we wonder why in this case (4 + 3) is the major product. We first studied a dipolar (4 + 3) cycloaddition pathway that would lead an oxyallyl cation tautomer of **2**, where the enol proton was transferred to the adjacent carbonyl, and **6** directly to **5** without an α -ketol rearrangement (Figure S2). However, the energy of this dipolar (4 + 3) transition state (**TS-S1**) is too high (29.7 kcal/mol) to be overcome under noncatalyzed conditions at room temperature.

We then investigated whether this potential energy surface indeed bifurcates to both products **4** and **5**. As demonstrated in our previous studies on post-transition state bifurcations of different types of pericyclic reactions, quasiclassical MD simulation is a powerful tool to explore bifurcating potential energy surfaces and to predict product ratios.^{34–39} To generate statistically significant results, we propagate a large amount of MD trajectories (>1000) on **TS1** structures employing the Grimme's GFN2-xTB quantum chemical method. The relative Gibbs free energies calculated using GFN2-xTB method are significantly different from those obtained with the ω B97X-D/6–31G(d,p) method (Figures 4a and S3); however, the force calculations employed by the ProgDyn program result in a similar dynamic ratio compared with those obtained with the ω B97X-D/6–31G(d,p) method (Figure S4) likely due to similar shapes in both potential energy surfaces after **TS1**, and both methods agreed with the experimental results (*vide infra*). The former method is more than 2000 times faster on our system than the latter and therefore holds great potential for full QM/MD simulation on large systems. Different implicit solvation models (GBSA toluene or water) were applied to simulate the experimental conditions. We performed normal-mode sampling of **TS1** and conducted MD simulations on **TS1** structure samples (Figure 4b). Analyzed from the **TS1** structure samples, the competing bond-forming distances of C3–C13 (bond 1) and C4–C13 (bond 2) are similar, which indicates **TS1** is ambimodal.⁴⁰ Analyzed from the trajectories (Figure 4d), the reaction pathway in both toluene and water⁴¹ does bifurcate after passing the **TS1** region and leads to either product **4** or **5**. The mainly dynamically concerted nature

of this cycloaddition is demonstrated by molecular dynamics studies, in which the average time gap between the formation of the first and second bond is 30 and 65 fs for **4** (Movie S1) and **5** (Movie S2), respectively (Figure 4c). The predicted distribution of **4/5** using xTB-MD is 30:1, while the experimental ratio is 30:5. This result agrees with our previous discovery and more recent example that the (4 + 2) product is always preferred to the (4 + 3) product.⁴² The large dynamic preference for **4** is associated with the steepness of the potential energy surface. As studied earlier by Singleton and co-workers, the shape of the potential energy surface influences reaction dynamics.^{43,44} The steepness of the slope likely affects the product ratio of **4** and **5**. The trajectory descends faster along the steeper side of a bifurcating surface due to a larger force, and therefore, this pathway is preferred. The other pathway requires a proton shift and is disfavored for that reason. The uneven product distribution is related to the nature of the bifurcating surface as illustrated in Figure 5. Figure 5a is a symmetric bifurcating surface with two products formed equally on the two sides of the valley ridge inflection. A representative class of reaction with this type of potential energy surface is an ambimodal homodimerization, such as the homodimerization of cyclopentadiene first studied by Caramella.⁴⁵ In the case an ambimodal reaction generates two different products, the bifurcating surface is unsymmetrical as illustrated in Figure 5b. The major product is the one located on the steeper side. The shape of each surface shown here is generated via an analytical function we derived, $Z = k[aX\sin(Y^2) + bY^2 + c\sin(X) + dXY]$, in which Z stands for potential energy, X is the bifurcating reaction coordinate, and Y is the perpendicular reaction coordinate.

xTB-MD simulations including water solvation resulted in the product distribution of **4/5** as 89:1 which is similar to the predicted ratio with toluene solvation; however, the experimental ratio of **4/5** is 1:3.4 using water as the reaction solvent. This disagreement suggests that the reaction must have proceeded differently in water. The α -keto-enol of **2** is acidic and will be ionized in water. The predicted pK_a of the enol hydroxy group of **2** is 5.2,⁴⁶ so that enolate anion (**2a**) of **2** is the major species in water at pH 7. We calculated the anionic pathway as shown in Figure 6a. The barrier height (**TS1c**, 19.7 kcal/mol) of the cycloaddition step is 2.2 kcal/mol lower in the anionic pathway than in the neutral pathway (Figure 2, *vide supra*). **TS1c** has a shorter bond-forming distance of C4–C13 (2.9 Å) compared with the competitive C3–C13 (3.1 Å), which suggests that **TS1c** may prefer the (4 + 3) product **5a**. Interestingly, the anionic cycloaddition is now of the inverse-electron-demand type, since the HOMO/LUMO gap of the diene–dienophile (10.4 eV) is higher than the dienophile–diene (7.8 eV), respectively; whereas the neutral cycloaddition is normal-electron-demanding [HOMO/LUMO gap of 8.2 eV (diene–dienophile) vs 10.0 eV (dienophile–diene)]. Thus, the reaction polarity is reversed by deprotonation of the dienophile. The anionic intermediate **5a** (5.0 kcal/mol) resulting from the cycloaddition is now higher in energy due to high basicity of a tertiary alkoxide anion. This anionic intermediate **5a** can undergo readily α -ketol rearrangement via **TS2c** (9.6 kcal/mol) that could lead to alkoxide **4a** (–10.1 kcal/mol), except that protonation of either **5a** or **4a** will occur readily because of the much higher pK_a s of the products, around 17. **TS1c** is ambimodal but will have a difference postbifurcating behavior because of its very different geometry from **TS1**.

We propagated xTB-MD trajectories based on the normal-mode sampling of **TS1c** using the xTB method (see Figure 6b). We found that 56% of the trajectories now lead to **5a**, representing the experimentally observed major product in water. The predicted dynamic ratio of **5a** and **4a** is 3.9:1 that is comparable to the experimental product ratio of **1** and **4** (3.4:1). The anionic cycloaddition is now dynamically stepwise, since the average time gaps between the formation of the two bonds are 211 and 203 fs for **4a** (Movie S3) and **5a** (Movie S4), respectively. Notably, a significant amount of entropic intermediate⁴⁷ was observed, which lies on a potential energy plateau preceding full formation of the second bond.³⁴ Although **5a** could undergo fast α -ketol rearrangement to **4a** due to the low barrier (4.6 kcal/mol), this is unlikely to happen in water, since a tertiary alkoxide such as **5a** or **4a** is instantaneously quenched by water upon generation, and therefore, the dynamic ratio of anion **5a** and **4a** represents the experimental ratio of the quenched products. In order to understand further how water molecules change the dynamic behavior of the reaction, we also performed MD simulations with the explicit solvation model, in which a TIP3P water⁴⁸ box was constructed around **TS1c**. As compared with the implicit solvation dynamics (Figure 6b), the cycloaddition reaction in explicit water (Figure 6c) starts with a complex with closer distance between **2a** and **6** due to the confined cavity for **TS1c**. The time gaps between the formation of the two bonds are 167 and 208 fs for **4a** (Movie S5) and **5a** (Movie S6), respectively. Less entropic intermediate is involved likely due to the reaction entropy being significantly reduced with restriction by the water cavity. The predicted dynamic ratio of **5a** and **4a** is 4.1:1. Thus, the overall process of the generation of **5** from **2** and **6** in water involves both anionic and neutral pathways: (1) ionization of dienophile **2** results in **2a**, (2) post-transition state bifurcation of ambimodal **TS1c** of the anionic pathway generates **5a** as the major species, (3) rapid protonation quenches alkoxide **5a** to form a thermodynamic well of the neutral reaction pathway, and (4) **5** is therefore trapped and isolated as the major product.

CONCLUSIONS

In summary, we have studied the dynamic effects that control the formation of natural products delitschiapyrone A and B. Delitschiapyrone A is not formed from the proposed Diels–Alder/ α -ketol rearrangement cascade but instead formed directly from a single cycloaddition reaction. Bifurcation of the reaction pathway from the ambimodal cycloaddition transition state results in both delitschiapyrone A and B. Delitschiapyrone B is intrinsic-dynamically preferred. Water changes this dynamic preference by favoring the deprotonated substrate. The dynamics then lead to the predominant formation of delitschiapyrone A. Nature has already developed a strategy to take advantage of ambimodal reactions to avoid overcoming high kinetic barriers and to control the periselectivity by proton transfer.

Supplementary Material

Refer to Web version on PubMed Central for supplementary material.

ACKNOWLEDGMENTS

We are grateful to the National Institute of General Medical Sciences, National Institutes of Health (GM 124480) and National Science Foundation (Grant CHE-1764328) for financial support of this research. All DFT calculations were performed on the Hoffman2 cluster at the University of California, Los Angeles, and the Extreme Science and Engineering Discovery Environment (XSEDE), which is supported by the National Science Foundation (Grant OCI-1053575).

REFERENCES

- (1). Luo J-G; Wang X-B; Xu Y-M; U'Ren JM; Arnold AE; Kong L-Y; Gunatilaka AAL Delitschiapyrone A, a Pyrone–Naphthalenone Adduct Bearing a New Pentacyclic Ring System from the Leaf-Associated Fungus *Delitschia* sp. FL1581. *Org. Lett* 2014, 16 (22), 5944–5947. [PubMed: 25365379]
- (2). Kurasawa K; Kwon E; Kuwahara S; Enomoto M Bioinspired Total Synthesis of Delitschiapyrone A. *Org. Lett* 2018, 20 (15), 4645–4648. [PubMed: 30003791]
- (3). Bannwarth C; Ehlert S; Grimme S GFN2-Xtb—An Accurate and Broadly Parametrized Self-Consistent Tight-Binding Quantum Chemical Method with Multipole Electrostatics and Density-Dependent Dispersion Contributions. *J. Chem. Theory Comput* 2019, 15 (3), 1652–1671. [PubMed: 30741547]
- (4). Viswanathan GK; Paul A; Gazit E; Segal D Naphthoquinone Tryptophan Hybrids: A Promising Small Molecule Scaffold for Mitigating Aggregation of Amyloidogenic Proteins and Peptides. *Front. Cell Dev. Biol* 2019, 7, 242. [PubMed: 31750300]
- (5). Alferova VA; Shuvalov MV; Korshun VA; Tyurin AP Naphthoquinone-derived polyol macrolides from natural sources. *Russ. Chem. Bull* 2019, 68 (5), 955–966.
- (6). Medentsev AG; Akimenko VK Naphthoquinone metabolites of the fungi. *Phytochemistry* 1998, 47 (6), 935–959. [PubMed: 9564730]
- (7). Medentsev AG; Akimenko VK Fungal naphthoquinone metabolites (Review). *Appl. Microbiol. Biotechnol* 1996, 32 (1), 7–29.
- (8). Medentsev AG; Arinbasarova AY; Akimenko VK Biosynthesis of naphthoquinone pigments by fungi of the genus *Fusarium*. *Appl. Biochem. Microbiol* 2005, 41, 503–507.
- (9). Foong LC; Chai JY; Ho ASH; Yeo BPH; Lim YM; Tam SM Comparative transcriptome analysis to identify candidate genes involved in 2-methoxy-1,4-naphthoquinone (MNQ) biosynthesis in *Impatiens balsamina* L. *Sci. Rep* 2020, 10 (1), 16123. [PubMed: 32999341]
- (10). Barrios-Gonzalez J; Perez-Sanchez A; Bibian ME New knowledge about the biosynthesis of lovastatin and its production by fermentation of *Aspergillus terreus*. *Appl. Microbiol. Biotechnol* 2020, 104 (21), 8979–8998. [PubMed: 32930839]
- (11). Auclair K; Sutherland A; Kennedy J; Witter DJ; Van den Heever JP; Hutchinson CR; Vederas JC Lovastatin Nonaketide Synthase Catalyzes an Intramolecular Diels-Alder Reaction of a Substrate Analogue. *J. Am. Chem. Soc* 2000, 122 (46), 11519–11520.
- (12). Mulder KCL; Mulinari F; Franco OL; Soares MSF; Magalhães BS; Parachin NS Lovastatin production: From molecular basis to industrial process optimization. *Biotechnol. Adv* 2015, 33 (6), 648–665. [PubMed: 25868803]
- (13). Witter DJ; Vederas JC Putative Diels-Alder-catalyzed cyclization during the biosynthesis of lovastatin. *J. Org. Chem* 1996, 61 (8), 2613–2623. [PubMed: 11667090]
- (14). Xu W; Chooi YH; Choi JW; Li S; Vederas JC; Da Silva NA; Tang Y LovG: The Thioesterase Required for DihydromonacolinL Release and Lovastatin Nonaketide Synthase Turnover in Lovastatin Biosynthesis. *Angew. Chem., Int. Ed* 2013, 52 (25), 6472–6475.
- (15). Mizushima Y; Kamisuki S; Kasai N; Shimazaki N; Takemura M; Asahara H; Linn S; Yoshida S; Matsukage A; Koiwai O; Sugawara F; Yoshida H; Sakaguchi K A Plant Phytotoxin, Solanapyrone A, Is an Inhibitor of DNA Polymerase β and λ^* . *J. Biol. Chem* 2002, 277 (1), 630–638. [PubMed: 11677229]
- (16). Chen S; Yu P; Houk KN Ambimodal Dipolar/Diels–Alder Cycloaddition Transition States Involving Proton Transfers. *J. Am. Chem. Soc* 2018, 140 (51), 18124–18131. [PubMed: 30479123]

- (17). Chai J-D; Head-Gordon M Long-range corrected hybrid density functionals with damped atom–atom dispersion corrections. *Phys. Chem. Chem. Phys* 2008, 10 (44), 6615–6620. [PubMed: 18989472]
- (18). Carpenter BK Nonstatistical dynamics in thermal reactions of polyatomic molecules. *Annu. Rev. Phys. Chem* 2005, 56 (1), 57–89. [PubMed: 15796696]
- (19). Ess DH; Wheeler SE; Iafe RG; Xu L; Çelebi-Öçülüm N; Houk KN Bifurcations on Potential Energy Surfaces of Organic Reactions. *Angew. Chem., Int. Ed* 2008, 47 (40), 7592–7601.
- (20). Hare SR; Tantillo DJ Post-transition state bifurcations gain momentum – current state of the field. *Pure Appl. Chem* 2017, 89 (6), 679–698.
- (21). Hong YJ; Tantillo DJ Biosynthetic consequences of multiple sequential post-transition-state bifurcations. *Nat. Chem* 2014, 6 (2), 104–111. [PubMed: 24451585]
- (22). Oyola Y; Singleton DA Dynamics and the Failure of Transition State Theory in Alkene Hydroboration. *J. Am. Chem. Soc* 2009, 131 (9), 3130–3131. [PubMed: 19215077]
- (23). Xu L; Doubleday CE; Houk KN Dynamics of 1,3-Dipolar Cycloadditions: Energy Partitioning of Reactants and Quantitation of Synchronicity. *J. Am. Chem. Soc* 2010, 132 (9), 3029–3037. [PubMed: 20148587]
- (24). Yang Z; Yang S; Yu P; Li Y; Doubleday C; Park J; Patel A; Jeon B.-s.; Russell WK; Liu H.-w.; Russell DH; Houk KN Influence of water and enzyme SpnF on the dynamics and energetics of the ambimodal [6 + 4]/(4 + 2) cycloaddition. *Proc. Natl. Acad. Sci. U. S. A* 2018, 115 (5), E848. [PubMed: 29348209]
- (25). Osuna S; Kim S; Bollot G; Houk KN Aromatic Claisen Rearrangements of O-Prenylated Tyrosine and Model Prenyl Aryl Ethers: Computational Study of the Role of Water on Acceleration of Claisen Rearrangements. *Eur. J. Org. Chem* 2013, 2013 (14), 2823–2831.
- (26). Liu F; Yang Z; Mei Y; Houk KN QM/QM' Direct Molecular Dynamics of Water-Accelerated Diels–Alder Reaction. *J. Phys. Chem. B* 2016, 120 (26), 6250–6254. [PubMed: 27092967]
- (27). Nishimura E; Ohfuné Y; Shinada T Total synthesis and structure elucidation of (±)-triumphalone and (±)-isotriumphalone. *Tetrahedron Lett.* 2015, 56 (3), 539–541.
- (28). Butler RN; Coyne AG Water: Nature's Reaction Enforcer—Comparative Effects for Organic Synthesis “In-Water” and “On-Water. *Chem. Rev* 2010, 110 (10), 6302–6337. [PubMed: 20815348]
- (29). Narayan S; Muldoon J; Finn MG; Fokin VV; Kolb HC; Sharpless KB On Water”: Unique Reactivity of Organic Compounds in Aqueous Suspension. *Angew. Chem., Int. Ed* 2005, 44 (21), 3275–3279.
- (30). See Figure S1 in the Supporting Information for the *exo* transition states.
- (31). Houk KN; Moses SR; Wu YD; Rondan NG; Jager V; Schohe R; Fronczek FR Stereoselective nitrile oxide cycloadditions to chiral allyl ethers and alcohols. The inside alkoxy effect. *J. Am. Chem. Soc* 1984, 106 (13), 3880–3882.
- (32). Raimondi L; Wu Y-D; Brown FK; Houk KN The “inside alkoxy effect” in intramolecular nitrile oxide cycloadditions: Ab initio and force field modeling. *Tetrahedron Lett.* 1992, 33 (31), 4409–4412.
- (33). Haller J; Niwayama S; Duh H-Y; Houk KN Stereoselective Diels–Alder Reactions of Hexachlorocyclopentadiene with Chiral Alkenes: New Insights Into the “Inside-Alkoxy” Model of Stereoselectivity. *J. Org. Chem* 1997, 62 (17), 5728–5731.
- (34). Yu P; Patel A; Houk KN Transannular [6 + 4] and Ambimodal Cycloaddition in the Biosynthesis of Heronamide A. *J. Am. Chem. Soc* 2015, 137 (42), 13518–13523. [PubMed: 26435377]
- (35). Xu L; Doubleday CE; Houk KN Dynamics of 1,3-Dipolar Cycloaddition Reactions of Diazonium Betaines to Acetylene and Ethylene: Bending Vibrations Facilitate Reaction. *Angew. Chem., Int. Ed* 2009, 48, 2746–2748.
- (36). Yang Z; Jamieson CS; Xue X-S; Garcia-Borràs M; Benton T; Dong X; Liu F; Houk KN Mechanisms and Dynamics of Reactions Involving Entropic Intermediates. *Trends in Chemistry* 2019, 1 (1), 22–34.
- (37). Liu F; Chen Y; Houk KN Huisgen's 1,3-Dipolar Cycloadditions to Fulvenes Proceed via Ambimodal [6 + 4]/(4 + 2) Transition States. *Angew. Chem., Int. Ed* 2020, 59 (30), 12412–12416.

- (38). Xue X-S; Jamieson CS; Garcia-Borràs M; Dong X; Yang Z; Houk KN Ambimodal Trispericyclic Transition State and Dynamic Control of Periselectivity. *J. Am. Chem. Soc* 2019, 141 (3), 1217–1221. [PubMed: 30623652]
- (39). Yang Z; Dong X; Yu Y; Yu P; Li Y; Jamieson C; Houk KN Relationships between Product Ratios in Ambimodal Pericyclic Reactions and Bond Lengths in Transition Structures. *J. Am. Chem. Soc* 2018, 140 (8), 3061–3067. [PubMed: 29419295]
- (40). Pham HV; Houk KN Diels–Alder Reactions of Allene with Benzene and Butadiene: Concerted, Stepwise, and Ambimodal Transition States. *J. Org. Chem* 2014, 79 (19), 8968–8976. [PubMed: 25216056]
- (41). See Figure S5 in the Supporting Information.
- (42). Zhang H; Novak AJE; Jamieson CS; Xue X-S; Chen S; Trauner D; Houk KN Computational Exploration of the Mechanism of Critical Steps in the Biomimetic Synthesis of Preisolactone A, and Discovery of New Ambimodal (5 + 2)/(4 + 2) Cycloadditions. *J. Am. Chem. Soc* 2021, 143 (17), 6601–6608. [PubMed: 33887906]
- (43). Thomas JB; Waas JR; Harmata M; Singleton DA Control Elements in Dynamically Determined Selectivity on a Bifurcating Surface. *J. Am. Chem. Soc* 2008, 130 (44), 14544–14555. [PubMed: 18847260]
- (44). Bogle XS; Singleton DA Dynamic Origin of the Stereoselectivity of a Nucleophilic Substitution Reaction. *Org. Lett* 2012, 14 (10), 2528–2531. [PubMed: 22540965]
- (45). Caramella P; Quadrelli P; Toma L An Unexpected Bispericyclic Transition Structure Leading to 4 + 2 and 2 + 4 Cycloadducts in the Endo Dimerization of Cyclopentadiene. *J. Am. Chem. Soc* 2002, 124 (7), 1130–1131. [PubMed: 11841256]
- (46). Predicted by using the ChemAxon program package.
- (47). Gonzalez-James OM; Kwan EE; Singleton DA Entropic Intermediates and Hidden Rate-Limiting Steps in Seemingly Concerted Cycloadditions. Observation, Prediction, and Origin of an Isotope Effect on Recrossing. *J. Am. Chem. Soc* 2012, 134 (4), 1914–1917. [PubMed: 22229840]
- (48). Jorgensen WL; Chandrasekhar J; Madura JD; Impey RW; Klein ML Comparison of simple potential functions for simulating liquid water. *J. Chem. Phys* 1983, 79 (2), 926–935.
- (49). Frisch MJ, et al. Gaussian 09, Revision A.02; Gaussian, Inc.: Wallingford CT, 2016. (For the full citation, please see Supporting Information).
- (50). Singleton DA; Hang C; Szymanski MJ; Greenwald EE A New Form of Kinetic Isotope Effect. Dynamic Effects on Isotopic Selectivity and Regioselectivity. *J. Am. Chem. Soc* 2003, 125 (5), 1176–1177. [PubMed: 12553813]
- (51). Ussing BR; Hang C; Singleton DA Dynamic Effects on the Periselectivity, Rate, Isotope Effects, and Mechanism of Cycloadditions of Ketenes with Cyclopentadiene. *J. Am. Chem. Soc* 2006, 128 (23), 7594–7607. [PubMed: 16756316]
- (52). Nieves-Quinones Y; Singleton DA Dynamics and the Regiochemistry of Nitration of Toluene. *J. Am. Chem. Soc* 2016, 138 (46), 15167–15176. [PubMed: 27794598]
- (53). Lu T gau_xtb: A Gaussian interface for xtb code. http://sobereva.com/soft/gau_xtb.

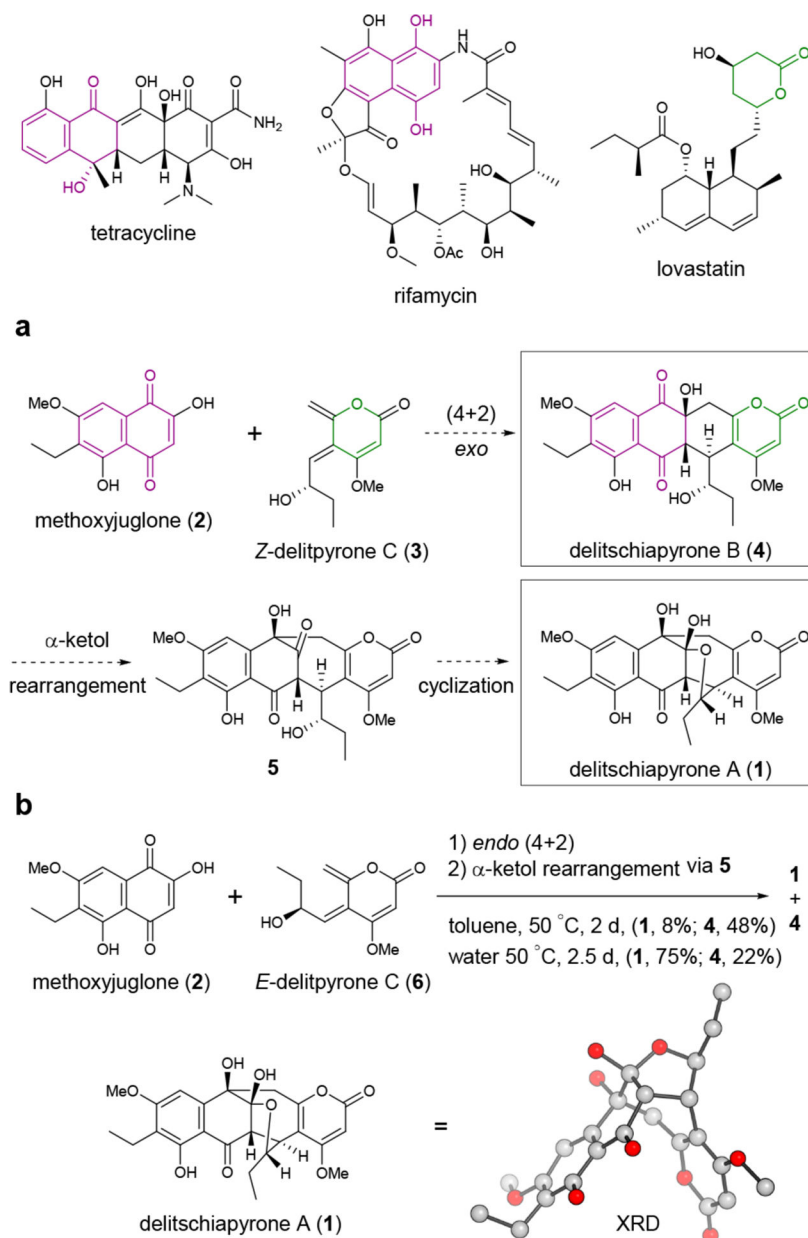


Figure 1. Representative naphthoquinone and 2-pyrone natural products and the structures of delitschiapyrone A (1) and delitschiapyrone B (2). (a) Proposed biosynthetic and (b) chemical synthetic pathways of delitschiapyrone A (1).

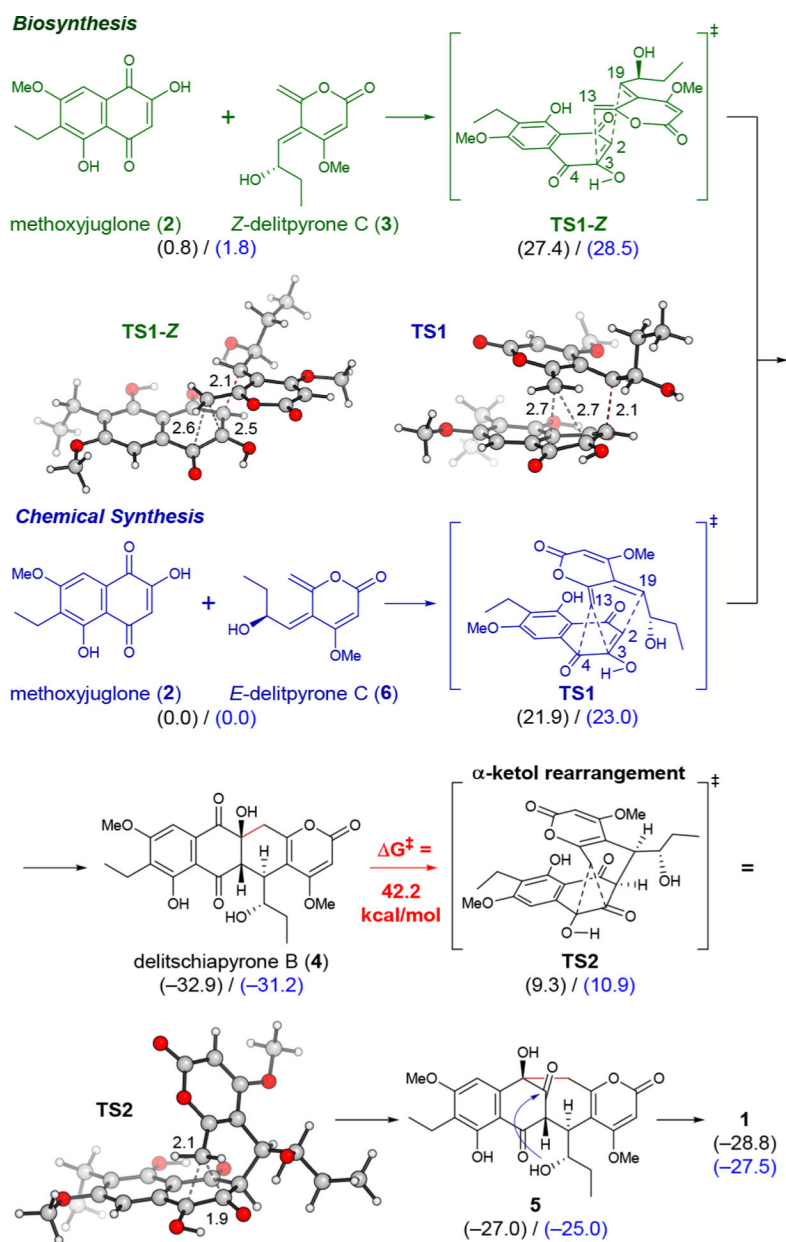


Figure 2. Calculated energies and structures of the transition states for different reaction pathways with ω B97X-D/6-31G(d,p)/CPCM(water or toluene, black/blue numbers, respectively). Free energies are in kcal/mol. The optimized geometries shown are in CPCM water.

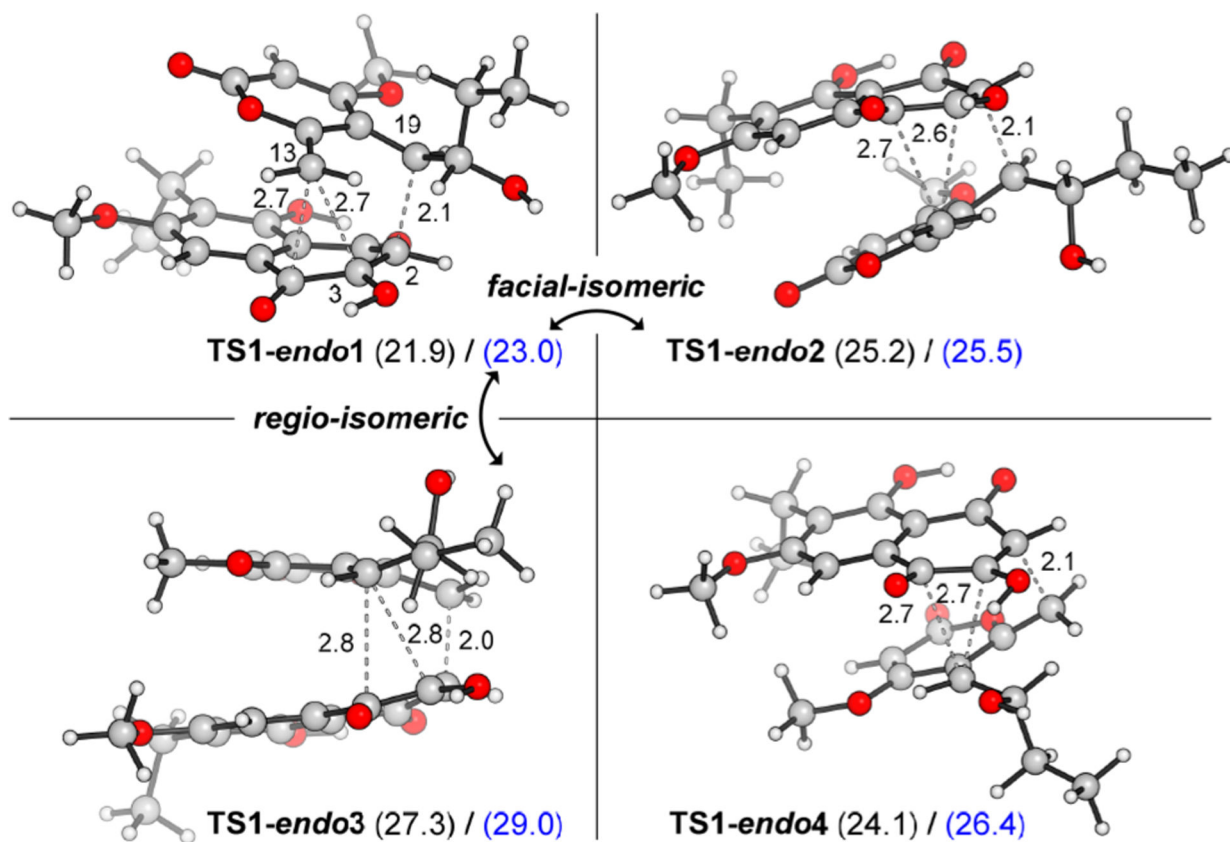
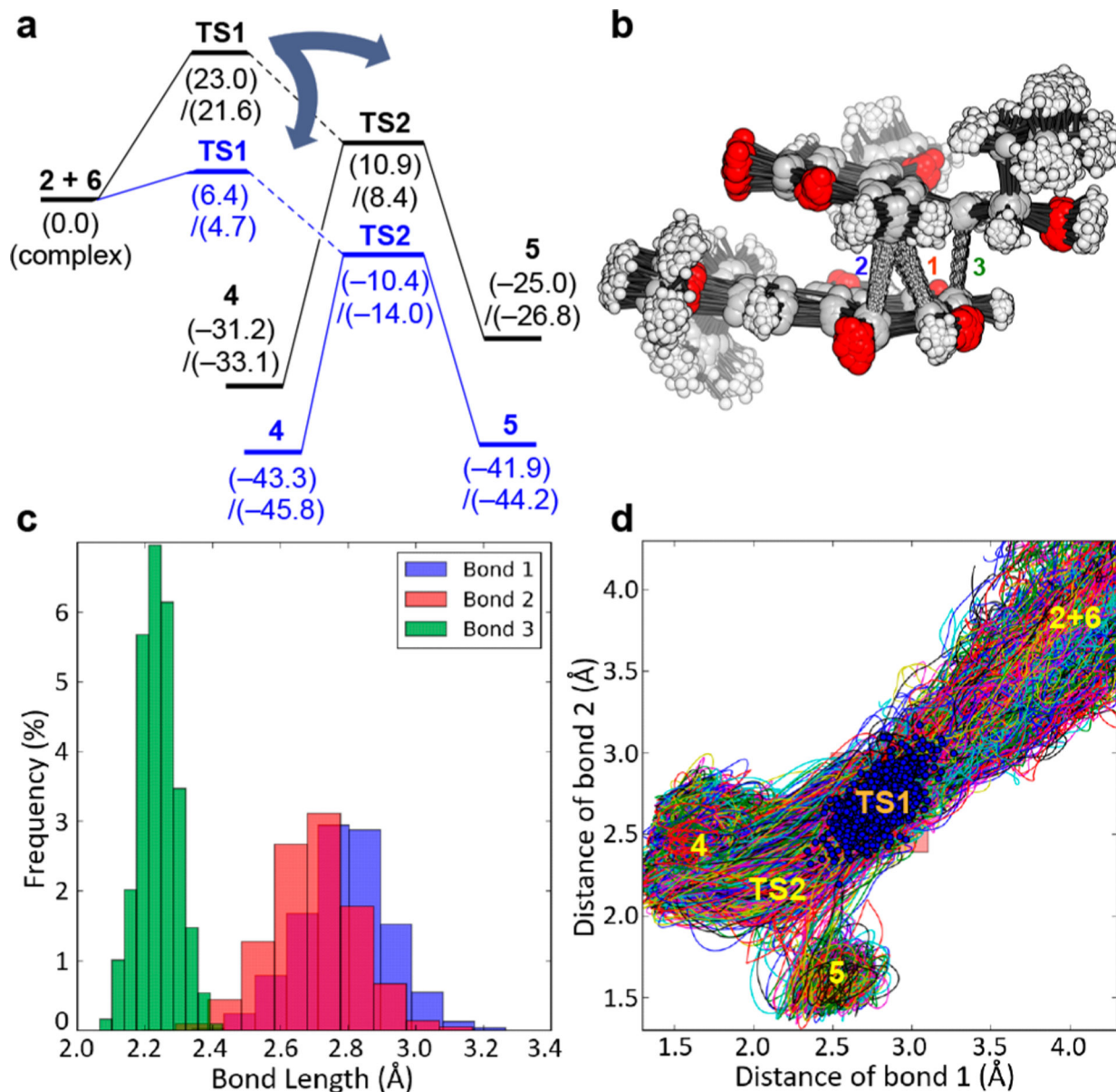


Figure 3. Stereoisomeric *endo* transition states. Free energies are relative to the reactive complex of **2** and **6** that leads to **TS1-endo1** and are in kcal/mol. The energies in black numbers are applying CPCM water solvation. The energies in blue numbers are applying CPCM toluene solvation. The optimized geometries shown are in CPCM water.

**Figure 4.**

Quasi-classic molecular dynamics simulation of TS1. (a) Schematic presentation of post-transition state bifurcation of **TS1** calculated with ω B97X-D/6-31G(d,p)/CPCM(toluene), numbers in black color, and GFN2-xTB(gas phase), numbers in blue color. The numbers in the front/back are free energies/enthalpies, respectively. (b) Overlaid normal-mode samples of the ambimodal **TS1** calculated with xTB and (c) distance distribution of the forming bonds 1, 2, and 3 in transition state structures calculated with xTB. (d) xTB-MD distance plot showing statistic distribution of the MD trajectories (1 ps) in GBSA toluene monitoring two bond forming distances and locations of key species along the reaction pathway. Bond 1 is the distance between C3 and C13, bond 2 is the distance between C4 and C13, and bond 3 is the distance between C2 and C19. Blue points are the locations of the normal-mode structural samples of **TS1**.

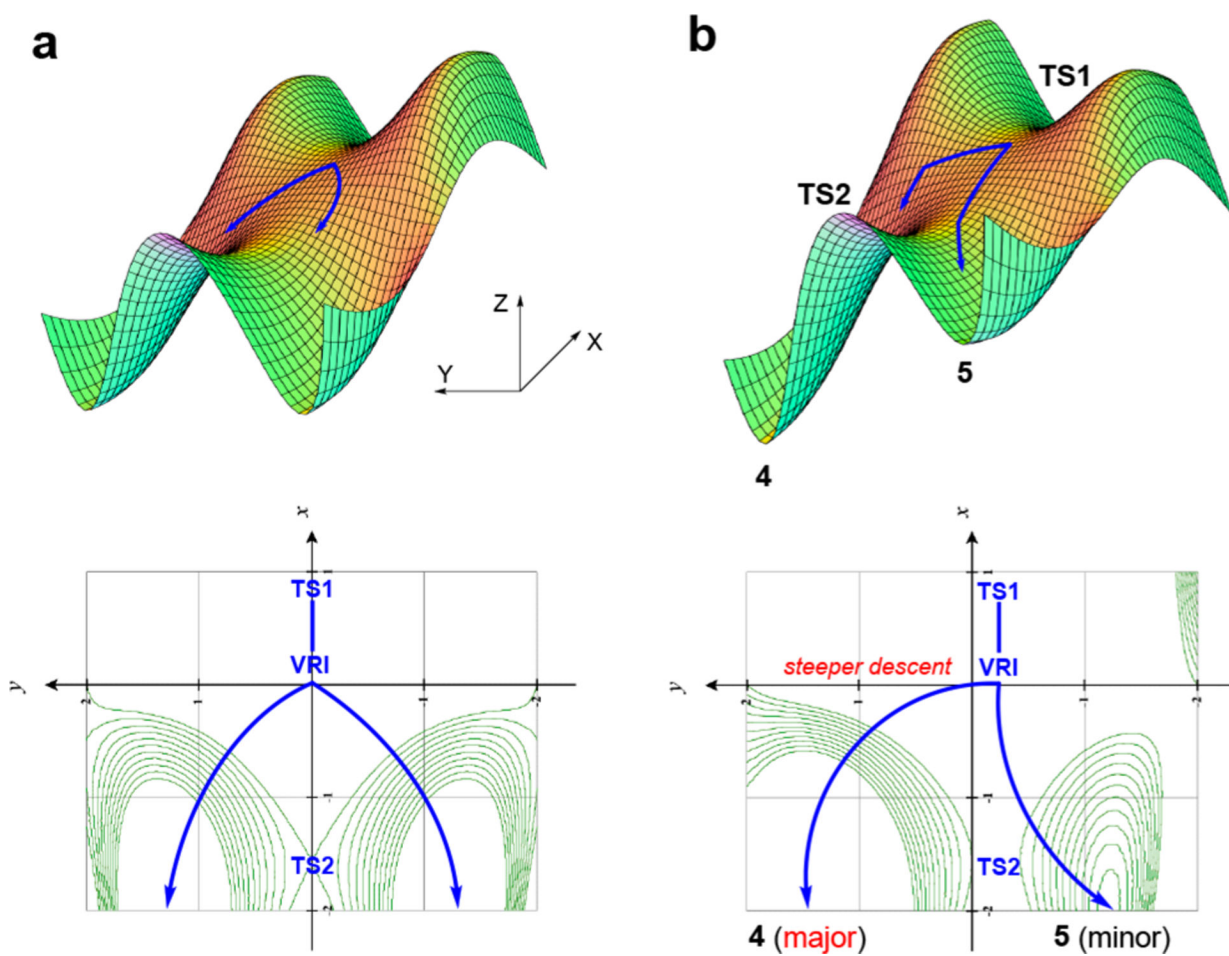


Figure 5. Two types of bifurcation surface. (a) Symmetrical bifurcation of the potential energy surface. (b) Asymmetrical bifurcation of the potential energy surface. The 2D plots are projections of the XY plane along Z axis with energy contours.

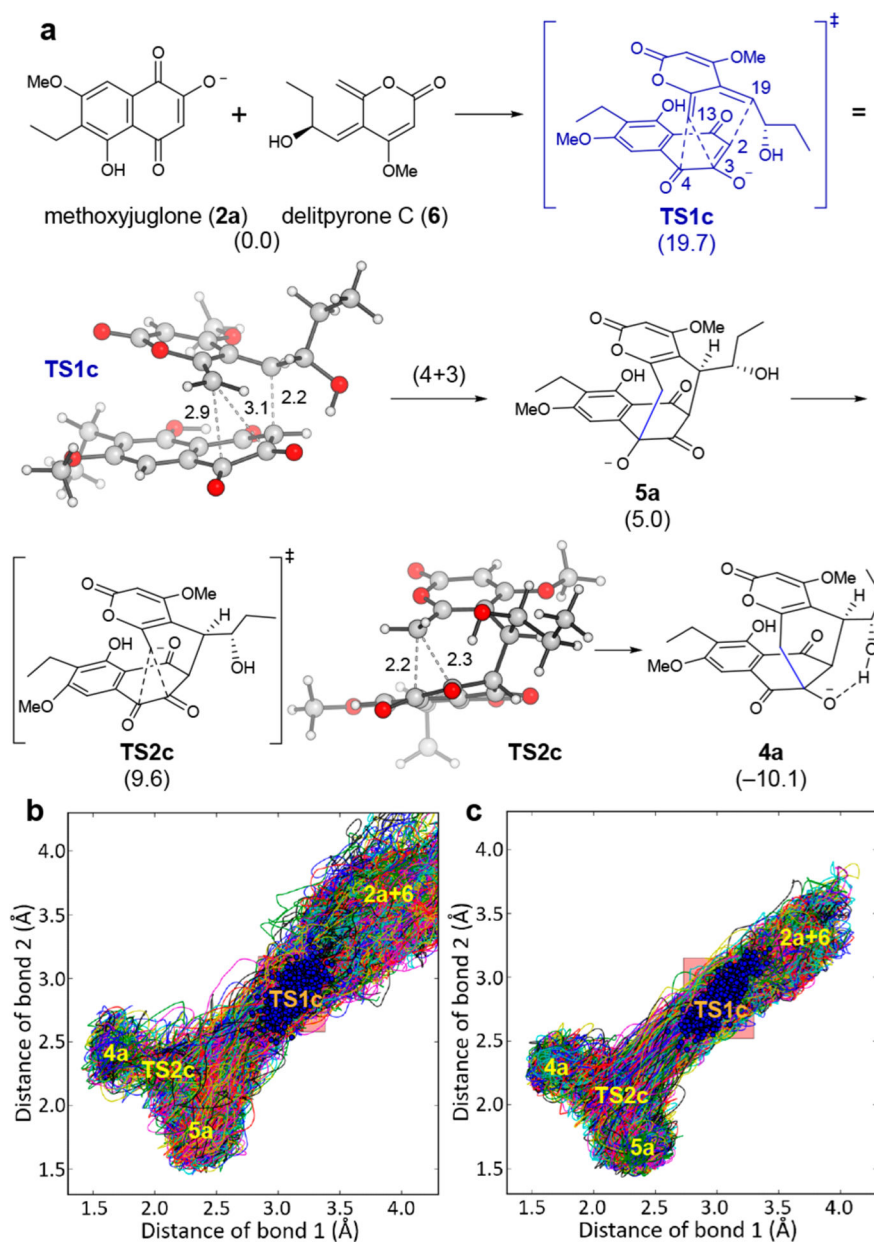


Figure 6. Anionic reaction pathway in water. (a) Calculated relative free energies and transition state structures with ω B97X-D/6-31G(d,p)/CPCM(water). (b) xTB-MD distance plot with implicit GBSA water solvation and (c) with explicit TIP3P water solvent box. Bond 1 is the distance between C3 and C13, and bond 2 is the distance between C4 and C13. Blue points are the locations of the normal-mode-sampled MD origins of **TS1c**. The red box is the transition state zone.